CubeSat Battery Thermal Analysis Using ESATAN

TESI DI LAUREA MAGISTRALE IN
SPACE ENGINEERING - INGEGNERIA SPAZIALE

Author: **Lorenzo Ambrosi**

Student ID: 920057
Advisor: Prof. Michèle Lavagna
Co-advisors: Matteo Quirino
Academic Year: 2021-22

Abstract

The approximations considered at the early stage of a thermal model make the initial simulations more efficient. A less accurate, but faster simulation is more useful for an initial thermal model. It is critical to find out what the key components from a thermal point of view are, as they are to be represented in the initial thermal model. In case some essential components for a space mission, as the CubeSat batteries, reached temperature close to the safety margins, it is necessary to perform a better thermal analysis by creating a more detailed model component, especially if the operative temperature windows are tight. This analysis will allow to check the accuracy of the initial temperatures and therefore the correctness of the approximations from an engineering point of view. This study is focused on the NanoPower BP4 batteries provided by GomSpace and used in the HERMES-TP mission. ESATAN is the software used to model the components and run the simulations. The new model is improved both from the geometry of the components, which are closer to reality, and the thermophysical properties of the materials. The cross-checking of the simulation results ran with both models, despite some differences, confirmed the accuracy of the initial approximations.

Keywords: battery, CubeSat, thermal model, approximation, ESATAN

Abstract in lingua italiana

Le approsimazioni effettuate nella fase iniziale di un modello termico servono a rendere le prime simulazioni più efficienti. È infatti preferibile per un modello termico iniziale poter effettuare simulazioni meno accurate, ma più veloci. Risulta quindi essere molto importante riuscire a determinare quali siano i componenti chiave dal punto di vista termico da rappresentare nel modello iniziale. Nel caso in cui alcuni componenti critici per una missione spaziale, com le batterie di un Cubesat, raggiungano temperature vicine a margini di sicurezza, è necessario approfondire l'analisi termica realizzando un modello più dettagliato del componente, in particolare se le finestre di temperatura operative risultano essere stringenti. Questa analisi permetterà di determinare se le temperature ottenute inizialmente siano corrette e che quindi le approssimazioni considerate in primo luogo siano idonee dal punto di vista ingegneristico. In questo studio sono state analizzate le batterie NanoPower BP4 fornite da GomSpace e utilizzate per la missione HERMES-TP. Il software utilizzato per il modello e per le simulazioni è ESATAN. Il modello più dettagliato si presenta migliorato sia dal punto di vista delle geometrie, più fedeli a quelle reali, sia dal punto di vista delle proprietà termo fisiche dei materiali. Il confronto dei risultati delle simulazioni compiute con il modello iniziale e quello più dettagliato, sebbene presenti alcune differenze, ha confermato la correttezza delle prime approssimazioni.

Parole chiave: batterie, CubeSat, modello termico, approssimazioni, ESATAN

Contents

List of Figures

List of Tables

List of Symbols

Variable	Description	SI unit
a	semi-major axis	km
A	surface area	mm^2
A_e	earth albedo	
α	absorptivity	
C_p	specific heat capacity	J/kg/K
δ	sun declination	deg
ΔT	temperature difference	K
ΔT_n	n-th temperature difference	K
e	eccentricity	
ϵ	emissivity	
Φ	scaling factor	
h	height	mm
h_c	cylinder height	mm
i	inclination	deg
k	thermal conductivity	W/m/K
l	width	mm
μ_c	discharge efficiency	
μ_d	discharge efficiency	
ω	argument of periapsis	deg
Ω	right ascension	deg
Ω_s	sun right ascension	deg
n	constant	

Variable	Description	SI unit
$\boldsymbol{\Psi}$	infra-red emission	
$\dot{\boldsymbol{Q}}$	thermal power	W
$\dot{\boldsymbol{Q}}_n$	n-th thermal power	W
$\boldsymbol{R}$	thermal resistance	K/W
$\boldsymbol{R}_c$	cylindrical thermal resistance	K/W
$\boldsymbol{R}_e$	external radius	mm
$\boldsymbol{R}_i$	internal radius	mm
$\boldsymbol{R}_l$	linear thermal resistance	K/W
$\boldsymbol{R}_n$	n-th thermal resistance	K/W
$\boldsymbol{\rho}$	density	kg/m^3
$\boldsymbol{t}$	thickness	mm
$\boldsymbol{T}_e$	earth temperature	K
$\boldsymbol{T}_s$	sun temperature	K
$\boldsymbol{\theta}$	true anomaly	deg

Nomenclature

ADCS	Attitude Determination and Control System
AOCS	Attitude and Orbit Control System
CAD	Computer-Aided Design
CC	Contact Conductance
CI	Conductive Interface
COTS	Component Off The Shelf
EPS	Electronic Power System
GPS	Global Positioning System
GRB	Gamma Ray Burst
Li-ion	Litium Ion
MLI	Multi Layer Insulation
Ni-Cd	Nickel-Cadmium
Ni-MH	Nickel-Metal Hydride
PCB	Printed Circuit Board
TCS	Thermal Control System
UDC	User Defined Conductor

1 | Introduction

1.1. What are batteries for?

From the beginning to the end of a mission, each satellite needs an electrical power supply to feed the rest of the satellite bus, all the on-board components and payloads.

The electronic power system (EPS) controls and coordinates the power flow. It controls the power produced by the primary source and it distributes the power from the storage units to the payloads. Typically, in the CubeSats, solar panels take the role of power generation and secondary batteries serve as energy storage.

The task of the battery is to provide power when the production from solar panels is not sufficient to cover the consumption. This is especially the case when a satellite passes through an eclipse and there is no light reaching the solar panels. If the battery is not able to fulfill this requirement, the result could be an interruption of the mission or even a loss of the spacecraft. Thus, the battery has a key role on every satellite and it is necessary to ensure its reliable operation in the space through the whole duration of the mission [5].

1.2. Lithium batteries

Among all the battery types available on the market, lithium ion batteries are known for their dense energy, longer lifetime, and rechargeable capacity. Since Li-ion batteries became commercially viable products in 1991, they have been adapted in multiple industrial applications, including the space industry [3].

The highlights of Li-ion battery characteristics include a wide range of operating temperatures, and a prominent working cycle. The systems are also capable of delivering short and high energy peaks without affecting the cell [3]. As reported in [5], lithium ion base batteries are the most used in space applications due to their significantly (2x-3x) energy and power density with respect to Ni-Cd and Ni-MH systems.

1.3.   Thesis work in HERMES

The HERMES-TP mission, in which my thesis is collocated, utilizes lithium ion batteries as energy storage. In order to verify that the batteries of the HERMES-TP stay within their operating temperature ranges, a thermal model of the satellite has been developed using ESATAN.

A first thermal simulation showed that during the mission the temperature reached by the batteries was very close to the higher temperature limit, not respecting the safety margins. For this reason, I improved the ESATAN model of the batteries to better understand if the problem related to the temperature was due to the excessive simplification during the first modeling of the battery package or if the temperature limits were not respected due to a design problem.

To do so, I started from the HERMES battery reference model and I improved the geometry of the components, the material used and the thermophysical properties of the materials. Finally, the results of the improved model showed that the battery is within the temperature operating limits with good margins, proving the sensitivity of the ESATAN model with respect to the different simplifications introduced in the original battery model.

Furthermore, it has been noticed that some cells of the battery package reached higher temperature with respect to the others. I focused on this problem and I presented some possible solutions to it.

2 | The Battery Model

This chapter is about the battery components and their model. I'll initially describe the main properties of the them. Then, a description of how the batteries were initially modeled is presented. Finally, I'll explain how I changed the battery model and the motivations of those modifications.

2.1. The NanoPower BP4

Figure 2.1: NanoPower BP4 from GomSpace.

As reported in the introduction, the batteries have a key role through the satellite mission. It is important to make sure that they can withstand the hostile environment encountered in space. Moreover, a suitable choice would be a component off the shelf (COTS) provided with flight heritage and extensive testing. For this reason, the batteries chosen for the HERMES mission are the NanoPower BP4 provided by GomSpace [1].

The NanoPower BP4 are made of an high capacity battery pack featuring four lithium ion cells. Depending on their configuration, the maximum capacity ranges from 2.6 to 5.2 Ah. In both configurations, the maximum available energy is 38.5 Wh [2].

Before describing in detail how the ESATAN model was carried out, let us see the main components of the NanoPower BP4.
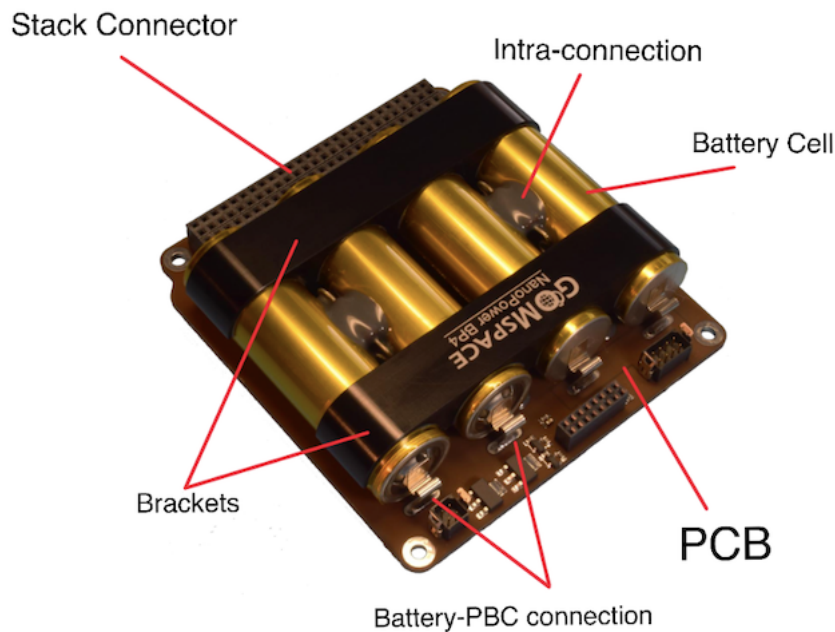
Figure 2.2: NanoPower BP4 components.

The most important component from the thermal analysis point of view are the four battery cells. They represent the core of the battery and for this reason, the ESATAN model would be focused on them in order to obtain results that are as much accurate as possible.

Then, there is the printed circuit board (PCB) where the four cells are attached to. In particular, the batteries are fitted to the board with Scotch-weld 2216 epoxy [2]. The PCB is also physically connected to the main structure of the satellite at the four corners, for this reason, it acts as a thermal sink for the batteries and it can also be considered as a thermal shield from the heat flow coming from the other on-board components.

The aluminum brackets which are glued to the batteries are also screwed to the PCB in order to add mechanical and thermal stability [2].

Finally, many types of connections are represented. In particular, the inter-cell connections are made with strips spot-welded to the cell terminals. The brackets are screwed to the PCB and are also glued to the batteries.

2.2. The initial HERMES battery model

In this chapter the main features of the initial ESATAN battery model are presented.
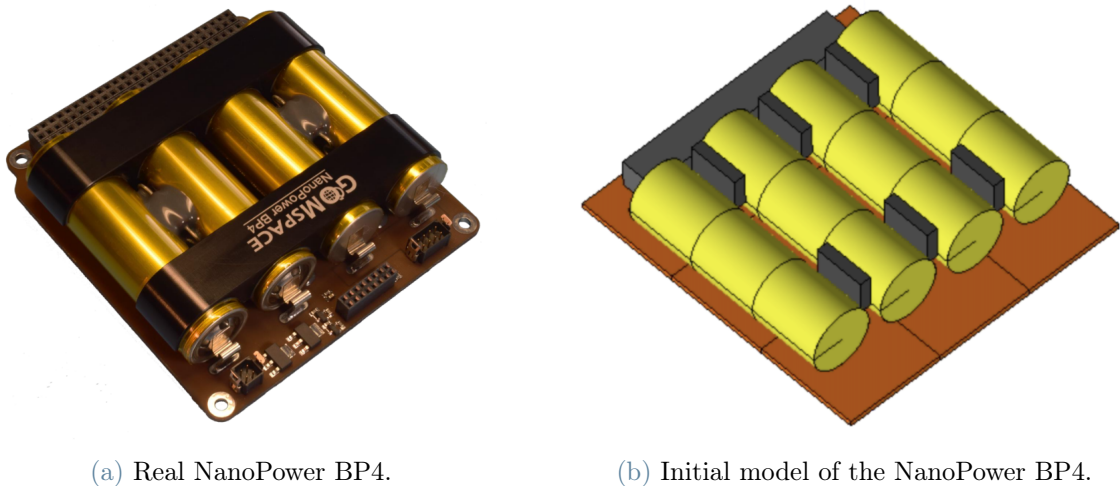
(a) Real NanoPower BP4.　　　　(b) Initial model of the NanoPower BP4.

Figure 2.3: Real and ESATAN representation of the NanoPower BP4.

The model originally created was a detailed but preliminary one. It contained the most relevant features of each component analyzed but with many geometrical simplifications. The main goal of the ESATAN model is to assess the temperature fields in the worst hot and cold cases for the different operating modes of the satellite. Secondly, the model is checking that all the components stay within their operating temperature limits [7]. The modeled components are:

- The cells
- The PCB and the stack connector
- The brackets
- The connections

2.2.1.   The cells

The four cells are the most interesting components for the simulations. For this reason, since the first ESATAN model they are represented as close as possible to the real ones. Their dimensions, which are taken from the CAD available at that GomSpace website, respect the real ones and are reported in Tab. 2.1.

Component	length [mm]	diameter [mm]
Cell	64.15	9.00

Table 2.1: Cells dimensions.

The thermophysical properties of the cells are taken from [7]. Moreover, as presented on the GomSpace data sheet, a layer of Kapton is modeled around the cells.

Name	k [W/m/K]	C_p [J/kg/K]	ρ [kg/m^3]	α	ϵ
Battery cell	70	495	3200	0.8	0.6

Table 2.2: Thermophysical properties of the cells.

The approximation from the geometry point of view concerns the edges of the cells. In ESATAN, they are modeled as perfect cylinders, while in reality the final part has some irregularities.

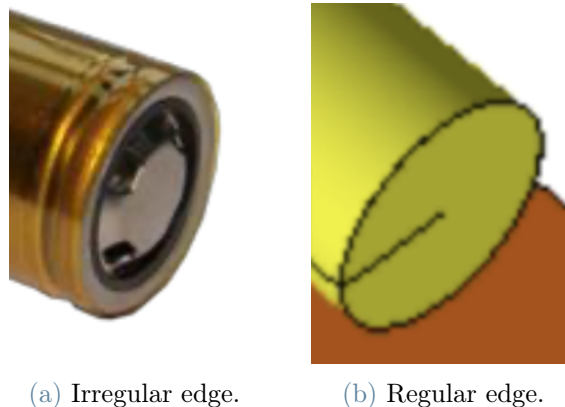(a) Irregular edge.   (b) Regular edge.

Figure 2.4: Real and ESATAN representation of the battery edge.

From an engineer point of view this approximation is considered acceptable since the majority of the heat exchanges will take place along the curved lateral faces of the cells.

Moreover, the irregular faces are connected to the base using the user defined conductors (UDC) this means that the conductive heat exchange from the battery to the PCB are correctly represented in the simulations.

UDCs are a tool available in ESATAN used to represent the connection between two different components in the model where a type of heat exchange takes place (advective, conductive, convective or radiative). To model a conductive connection, it is required to compute the thermal resistance of the conductor. As an example, let us compute the thermal resistance of the conductors connecting the front face of the cells to the PCB. Given the dimension of the conductor and its thermal conductivity k [W/m/K], it is possible to compute the thermal resistance by using the following equation:

$$R_l = \frac{t}{kA} \tag{2.1}$$

where R_l is the thermal resistance, t the distance between the two components and A is the section area of the conductor, which is considered constant. An example of it is showed in Fig. 2.5. A better explanation about the modeling of the UDCs is given in section 2.3.4.

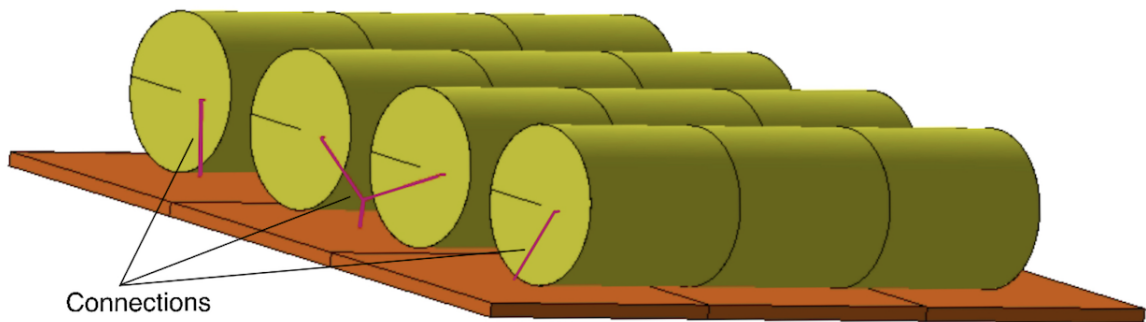Figure 2.5: Red lines representing the connections.

From the mesh point of view, the solid is divided into 3 parts. It has been assumed that the cells have homogeneous thermal properties, thus an higher discretization would not bring better results.

Finally, for what concerns the collocation of the cells and the distance between them, the reference values are taken again from the CAD model available.

2.2.2.   The PCB and the stack connector

The PCB is the board where the four cells are allocated. It is also directly connected to the main structure of the CubeSat at the four edges.

In this case, the approximation is clear: the majority of the components on the PCB are not modeled in ESATAN model. This choice is due to the fact that the thermal relevance of a component can be classified based on the power dissipated, its thermal inertia, its material properties like thermal conductivity and heat capacity, and connections to other parts of the CubeSat. The dissipated power and thermal interfaces are regarded as most critical. The designs of the thermally relevant components are simplified based on identification of the parts that have a large heat capacity, dissipate power, or have thermal connections to other parts of the satellite [8].

In the NanoPower BP4 PCB, the only modeled element is the stack connector which provides electrical connections between PCBs. It mostly consists of plastic, but more than 100 metal pins offer a way of heat transfer between PCBs on top of their purpose of electrical connection [8].

The thermophysical properties of the PCB are represented in Tab. 2.3.

Name	k **[W/m/K]**	C_p **[J/kg/K]**	ρ **[kg/m^3]**	α	ϵ
PCB	20	589	2223	0.80	0.60
Stack connector	175	900	2770	0.88	0.76

Table 2.3: Thermophysical properties of the PCB and the stack connector.

The mesh also in this case is poor. The board is divided into nine squares since it is assumed that the properties of the board are homogeneous.

Finally, it can be noticed that the holes are not considered, both for the stack connector, the screws for the brackets and for the connection with the main structure. There are mainly two reasons for this choice. The first one is that the holes generation in the solids slows the software down. For the reference model, it is preferred a less accurate but faster and more efficient simulation. Moreover, the holes can generate singularities during the simulation and as a result the simulations are not reliable. The second reason is that the connection with the rest of the structure are modeled using the UDCs or contact resistances (stack connector-PCB, brackets-PCB).

2.2.3.   The brackets

The brackets are mainly needed to add mechanical and thermal stability to the battery pack. For the initial thermal analysis, only the vertical components are modeled. They are placed between the batteries and they start from the PCB and move along the sides of the batteries. The reason behind this simplification is that the brackets do not generate heat. However, since they are made by aluminum, they carry heat fast. They gather heat from the batteries and they transmit it via conduction directly to the PCB. Moreover, their lateral surface is not negligible from the heat exchange point of view.

To loyally represent the optical properties of the brackets, reported in Tab. 2.4, it is considered a layer of black painting. Moreover, since the batteries are glued to the brackets, UDCs are utilized to model the connection.

This time, to model the thermal resistance of the glue around the cells, a cylindrical resistance model is considered. To do so, the following equation is used:

$$R_c = \frac{1}{(2\pi h_c k)} \ln(R_e/R_i) \tag{2.2}$$

where h_c is height of the cylinder, k is the thermal conductivity of the glue and R_e and R_i are the length of the external and internal radius of the glue respectively. They are represented by the red lines in Fig. 2.6.
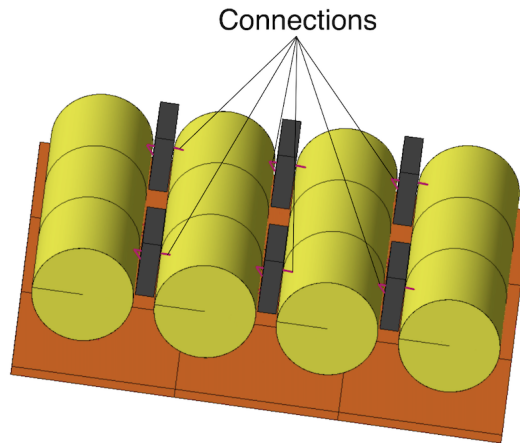
Figure 2.6: Example of UDCs.

Also in this case, a better explanation about the modeling of the UDCs is given in section 2.3.4.

Their thermal properties are summarized in Tab. 2.4

Name	k [W/m/K]	C_p [J/kg/K]	ρ [kg/m³]	α	ϵ
Brackets	120	824	2724	0.88	0.76

Table 2.4: Thermophysical properties of the brackets.

2.2.4.   The connections

Some connections have already been presented through the UDCs. However, ESATAN offers another option to define how two components can exchange heat, the conductive interfaces (CI), highlighted in orange in Fig. 2.7.

Figure 2.7: An example of conductive interfaces.

The CI are automatically computed by ESATAN, however the value of the contact conductance can be chosen manually. To complete the thermal network related to the NanoPower BP4, Tab. 2.5 summarizes the elements connected, the type of connection and the thermal resistance or contact conductance (CC).

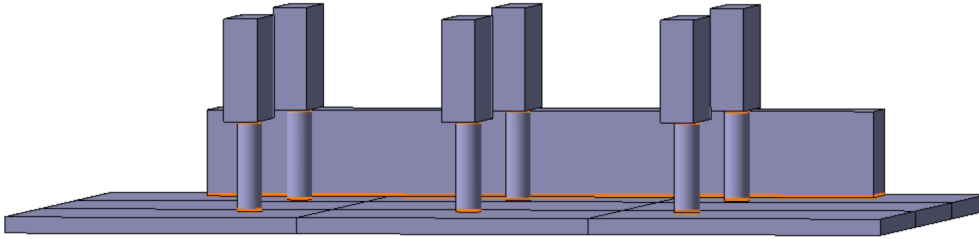| Element A	Element B	Type	R [W/K]	CC [W/m²/K]
Cell front face	PCB	UDC	33.33	-
Cell middle face	PCB	UDC	3.85	-
Cell face 1 & 3	Bracket	UDC	0.02	-
Cell face 1 & 3	Bracket	UDC	0.04	-
BP4 PCB	GPS PCB	UDC	5.95	-
BP4 PCB	Dock EPS	UDC	0.74	-
Bracket	Bracket support	CI	-	100
PCB	Bracket support	CI	-	100
PCB	Stack connector	CI	-	100

Table 2.5: Connection properties.

2.3. The enhanced battery model

At this point of the design, the results of the simulations done with the initial model are available. From them it is possible to highlight two modes which are the most critical one from the thermal point of view. These modes are the OBS and COMM-DATA.
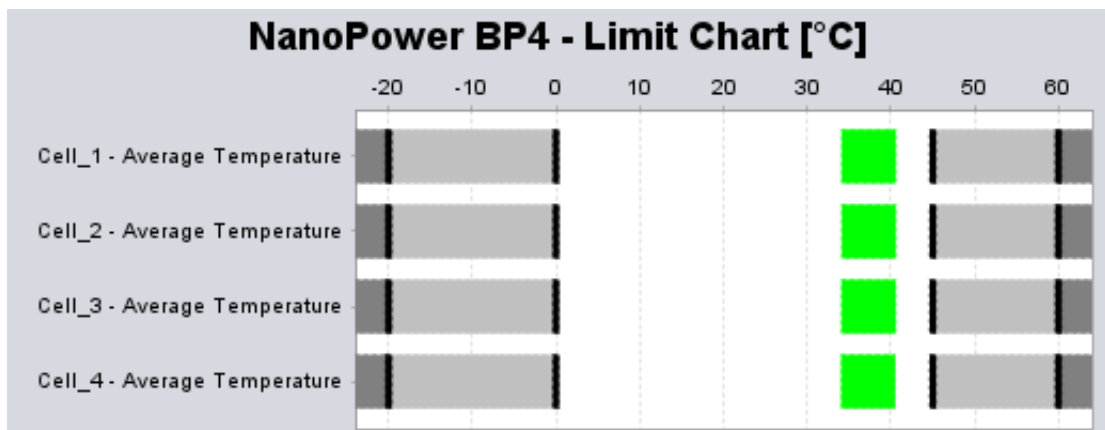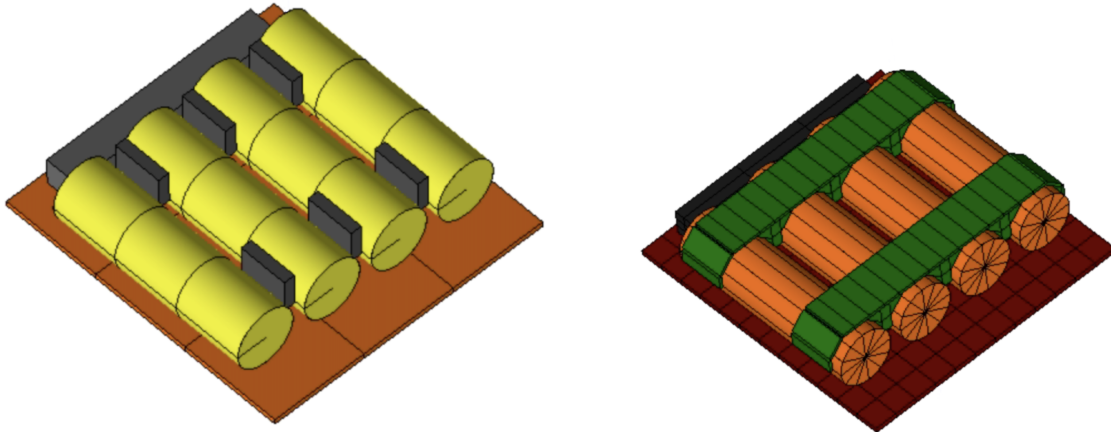

Figure 2.8: NanoPower BP4 limit chart, initial model.

These two modes will be analyzed with the enhanced model to better understand if the temperature limits are not respected due to an excessive simplification of the model or due to a design problem.

Let us now move to the enhanced battery model.

(a) Initial model of the NanoPower BP4.   (b) Enhanced model of the NanoPower BP4.

Figure 2.9: Initial and enhanced ESATAN representation of the NanoPower BP4.

The enhanced model is similar to the initial one, but it contains more information. The components analyzed are the same, but they are more refined in therms of geometry. Moreover, a better analysis is carried out to gather more information about the materials and their thermal properties. The goal of this refinement is to obtain results that are as much as possible close to the reality.

Let us now break down again the model components and see how the new characteristics can influence the results.

2.3.1. The cells

Starting from the cells, they are again the main focus during the simulation. This time, the mesh is more refined: the discretization is higher and it is oriented radially, dividing the cells in 12 slices. The reason behind this discretization is that this way it is possible to better analyze the region of the cells where there are connection with the other components of the battery pack. In particular, the connection with the PCB, the brackets and the cell-to-cell connection (between the two cells on the right and the two cells on the left, as visible in Fig. 2.2). Also the thermal properties of the material are slightly different as reported in Tab. 2.6.

Name	k [W/m/K]	C_p [J/kg/K]	ρ [kg/m^3]	α	ϵ
Battery Cell	130	960	2810	0.8	0.6

Table 2.6: Thermophysical properties of the enhanced battery cells.

Concerning the dimensions and the collocation on the board, the values used are the one available on the GomSpace CAD.

2.3.2. The PCB

For what concerns the PCB, also in this case, the greatest difference is in the mesh discretization. This time, the higher discretization can help in understanding the heat flux directions and in identifying the hotter areas that might need to be cooled or the other way around, the cooler areas could be used as thermal sinks. Moreover, also in this case, the better discretization helps in analyzing the areas where the conduction exchanges take place. In particular, the one between the PCB and the cells. Finally, while the stack connector properties are the same, the PCB ones are slightly different as reported in Tab. 2.7.

Name	k [W/m/K]	C_p [J/kg/K]	ρ [kg/m^3]	α	ϵ
PCB	28.25	910	2346	0.80	0.60
Stack connector	175	900	2770	0.88	0.76

Table 2.7: Thermophysical properties of the enhanced PCB and the stack connector.

2.3.3. The brackets

Let us know focus on the brackets. They are the components which changed the most. As reported in Fig. 2.9, their geometry is now closer to the reality. With respect to the initial model, the lower part of them, which is connected with the PCB, is different: in the enhanced model the difference between the bracket part and the support, the screw, is clear. They are represented as different components with different thermophysical properties, which are summarised in Tab. 2.8. Moreover, the top part of the bracket is added to the model. This is done, not only to make the model closer to the reality, but also because they can be considered relevant elements both during the radiative heat exchanges, given the dimension of their side surface, and conduction exchanges since they are made of aluminum.

Name	k [W/m/K]	C_p [J/kg/K]	ρ [kg/m^3]	α	ϵ
Brackets	130	960	2810	0.88	0.76
Screw	120	824	2724	0.88	0.76

Table 2.8: Thermophysical properties of the brackets and screw.

2.3.4.   The connections

Finally, the connections. In the new model they are the elements that required more research. As a matter of fact, they are the components with the higher level of uncertainty.

To model the connections between two components of the satellite, or in this case the battery package, two different methods are used in ESATAN. These are the CIs and the UDCs. Some example of them have already been presented in previous chapters. However, in this chapter a better and more detailed explanation on how to compute them will be given.

Let us start by saying that there are different types of heat exchange. One of them is conduction, in other words is the type of heat exchange that take place when two solids are physically connected and it is possible to identify a contact surface. The UDCs in ESATAN are used to define from the thermal point of view how the two solids exchange heat.

For what concerns the CIs, ESATAN can automatically compute them. However, the value of the contact conductance can be chosen manually.

In the enhanced model, the CIs are used to define the following contact surfaces, which are highlighted in Fig. 2.10:

- PCB - stack connector
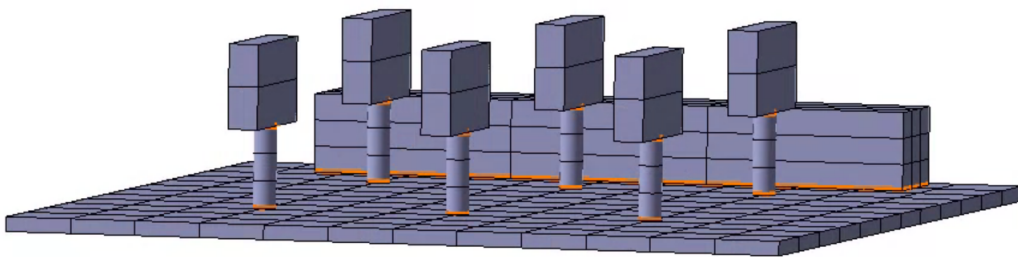
- PCB - screw

- bracket - screw

Figure 2.10: Contact interfaces highlighted in orange.

in all of them the thermal conductance value is 100 W/m²/K [4].

Regarding the UDCs, they represent the material connecting two components, such as the

glue between the cells and the brackets or the spacers which connects the battery PCB to the main structure of the satellite. By defining their properties, in particular the thermal transmittance, the features of the heat exchange are defined.

It must be pointed out that ESATAN works with the thermal transmittance to define the properties of the UDCs. However, for the sake of simplicity, it will now be presented a deeper explanation about the computation of the thermal resistances, which are the inverse of the thermal transmittances.

The thermal resistance associated to a solid is an indicator of how the solid resist to a conductive heat flow. In particular, in the case of materials in steady state condition without internal heat generation, the thermal resistance links the power which flows through the material and the different temperatures at two points of it with the following relation [6]:

$$\dot{Q} = \frac{\Delta T}{R} \tag{2.3}$$

where $\dot{Q}$ is the thermal power flow, ΔT is the temperature difference and R is the thermal resistance.

There are two types of thermal resistance used in the enhanced model:

- the linear resistance, R_l

- the cylindrical resistance, R_c

To compute the linear thermal resistances R_l, three geometrical quantities (the width, l, the height, h, and the thickness, t) and the thermal conductivity, k, are required. Then, the following equations are used:

$$A = h\,l \tag{2.4}$$

$$R_l = \frac{t}{k\,A} \tag{2.5}$$

on the other hand, to compute the cylindrical thermal resistances R_c, the height of the cylinder, h_c, the internal radius R_i and the external radius R_e together with the thermal conductivity, k, are required. Then, the following equation is used:

$$R_c = \frac{1}{(2\pi h_c k)} \ln(R_e/R_i) \tag{2.6}$$

All the thermal resistances computed in the model, can be divided into the following groups:

- linear

  - cell-cell

  - bracket-bracket

  - front cell-PCB

- cylindrical

  - cell-PCB

  - cell-bracket

Fig. 2.11 shows the cell-cell connection. In this case, a linear resistance is considered. The material is aluminum. The parameters used to compute the value of the resistance are showed in Tab. 2.9.

Fig. 2.12 shows the links between the brackets components. Also this time a linear resistance is considered. The material is aluminum, and the connection is required since in the model the curved parts of the brackets are divided into two separated pieces, while in reality the whole bracket is made by a single piece. The parameters used to compute the value of the resistance are showed in Tab. 2.9.

Fig. 2.13 shows the connections between the front face of the cell and the PCB. Due to the mesh, 12 linear resistances are computed. The material is aluminum. The parameters used to compute the value of the resistance are showed in Tab. 2.9.

Fig. 2.14 represents the connections between the bottom part of the cell and the PCB. This time a cylindrical resistance is modeled. The material is the Scotch-Weld 2216 Epoxy. The parameters used to compute the value of the resistance are showed in Tab. 2.10.

Finally, Fig. 2.15 shows the cell-bracket connection. Also this time cylindrical resistances are considered to model the Scotch-Weld 2216 Epoxy that glues the cells to the brackets. The parameters used to compute the value of the resistance are showed in Tab. 2.10.
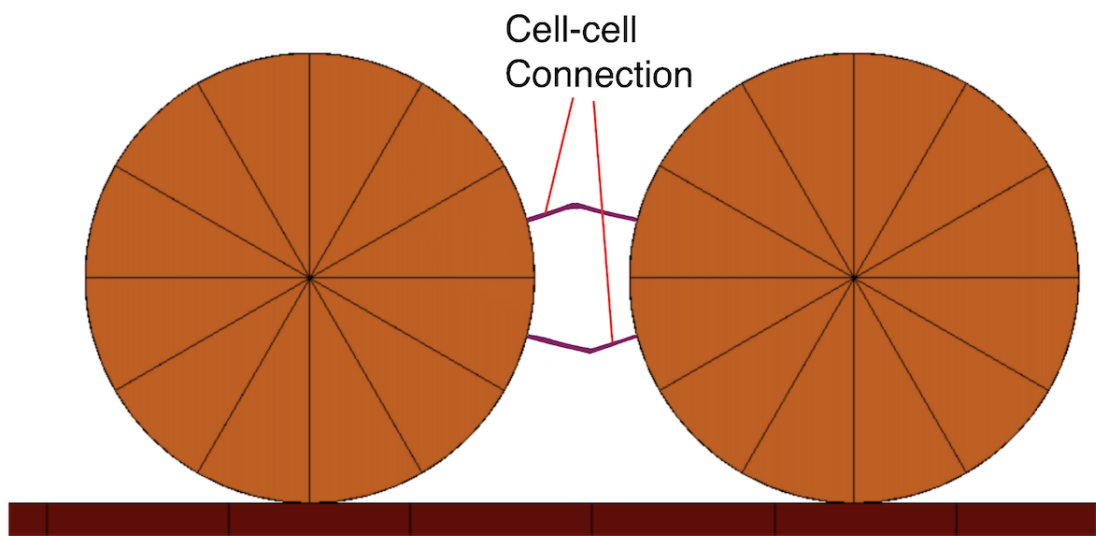
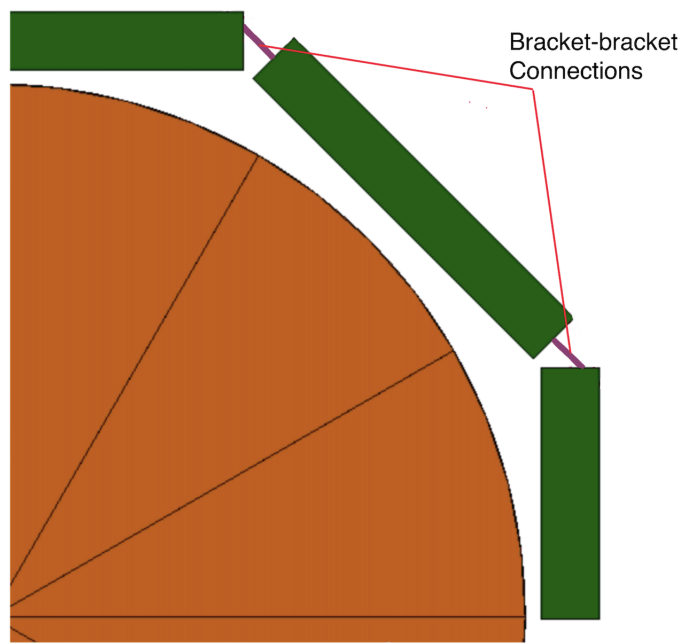Figure 2.11: Cell - cell connection.

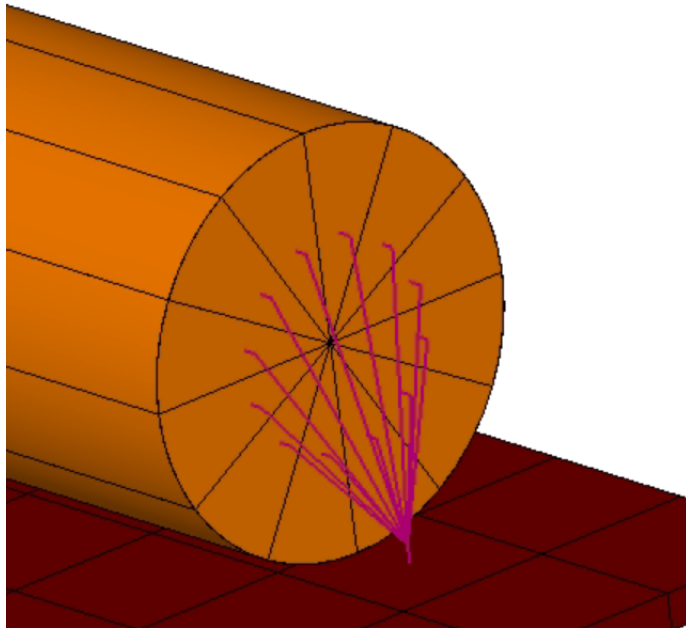Figure 2.12: Bracket - bracket connection.

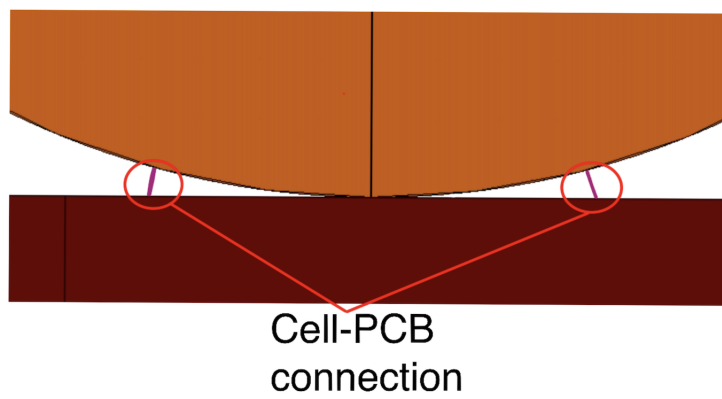Figure 2.13: Cell front face - PCB connection.

Figure 2.14: Cell - PCB connection.
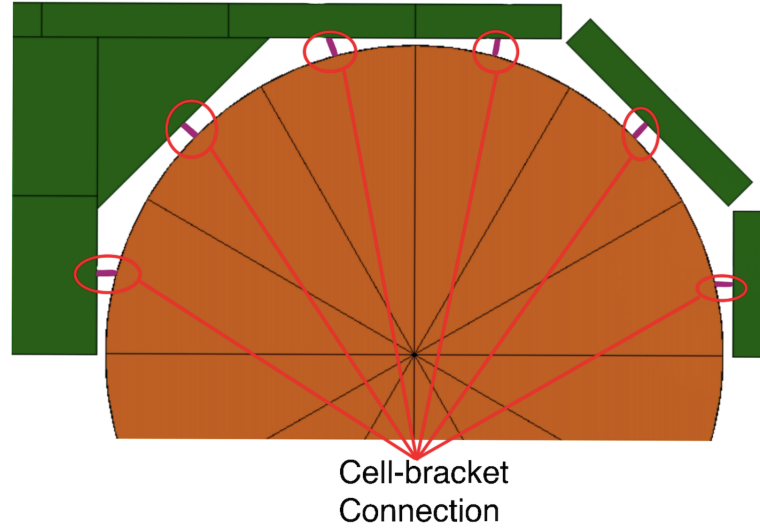
Cell-bracket
Connection

Figure 2.15: Cell - bracket connection.

Now, due to the higher definition in the meshes of the NanoPower BP4 components, the number of UDCs created to represent the thermal network has increased to more than 70. Moreover, due to the higher discretization, the computed resistance (R_l, R_c) must be multiplied by a scaling factor, ϕ.

To better understand what is the role of the scaling factor, let us consider the thermal resistance of a cylinder.

Referring to equation 2.3, if $\dot{Q}$ and ΔT are known, R can be easily computed. This R is the relation between the heat flowing through the whole cylinder volume. So, what would be the thermal resistance associated to a slice of the cylinder? If we suppose that the cylinder is divided into n equal slices, and that through each slice flows the same $\dot{Q}_n$, it is correct to say that

$$n\dot{Q}_n = \dot{Q} \tag{2.7}$$

where $\dot{Q}_n$ is the thermal power flowing through each slice and $\dot{Q}$ is the thermal power flowing through the whole cylinder. If we also suppose that the temperature difference of each slice, ΔT_n is equal to the total temperature difference, ΔT, so

$$\Delta T_n = \Delta T \tag{2.8}$$

By substituting 2.7 and 2.8 inside 2.3 it is possible to find that

$$R_n = nR \tag{2.9}$$

this means that the thermal resistance, R_n, associated to one single slice of the cylinder is equal to n-time the thermal resistance, R, associated to the whole cylinder. n is the scaling factor. In a similar fashion, it is possible to compute the same results for the linear case, when the surface is divided into n equal smaller surfaces.

Let us now look at an example for the battery:

Consider the cell-PCB connection. In this case the thermal resistance is cylindrical and is simulating the glue between the battery cell and the PCB, as showed in Fig. 2.14.

The scaling factor ϕ takes into account that the connection takes places between a single slice of the mesh of the battery cell and a single square of the mesh of the PCB. In this case, since the total slices of the cells are 12 and the squares of the PCB considered to be in contact with the cell are 8, the scaling factor is equal to 96.

Elements	l [mm]	h [mm]	t [mm]	k [W/m/K]	ϕ	R_l [K/W]
Bracket - Bracket	15	0.98	1.0	130	1	49.74
Cell - Cell	12.83	4.71	3.8	120	1	0.52
Front face cell - PCB	6	0.50	12	130	12	378.46

Table 2.9: Parameters and linear resistances.

Elements	l [mm]	R_i [mm]	R_e [mm]	k [W/m/K]	ϕ	R_c [K/W]
Cell - PCB	64.15	9	9.25	0.0164	96	397.91
Cell - Bracket	15	9	9.25	0.0164	12	212.72

Table 2.10: Parameters and cylindrical resistances.

3 | The HERMES model

This chapter is about the HERMES mission. It described the main goal of it and explain why a thermal analysis of the model is required at any stage of the design. Then, the second section focuses on how the ESATAN model is built. Finally, it is explained how the enhanced battery model is collocated inside the satellite and how it interacts with the other modeled components.

3.1. The HERMES mission

The HERMES-TP mission is a constellation of three CubeSats of 3U size with the main goal of detecting and triangulating Gamma Ray Bursts. The mission is a technological path finder (TP) for the HERMES- SP mission that aims at integrating HERMES-TP with other three CubeSats of the same type thus creating a constellation of six CubeSats. The detection of the Gamma Ray Burst is actuated by a scientific payload manufactured by INAF. The payload is able to detect the time of occurrence of the observation and it is able to record the energy time evolution of the event. As soon as the payload detects a burst, the time of the detection and the satellite position are sent back to Earth using a link to the GlobalStar constellation. The prompt communication of the GRB detection enables the spreading of an alarm through the telescope networks, such as the GCN, providing better chances to observe the phenomena with different space segments. Politecnico of Milano is in charge of the design of the service module of the mission as well as the integration of the INAF payload into the service module. The design involves the selection of all the hardware needed as well as its configuration inside the module, integration and testing. The success of the design involves the coordination of many subsystems and among them the thermal control subsystem (TCS). The TCS has the straightforward goal to keep all the components in their operating temperature ranges throughout the mission duration. To do so, a thermal model of the 3U HERMES-TP CubeSat is created in ESATAN. The main goal of the ESATAN model is to assess the temperature fields in the worst hot/cold cases for the different operating modes of the satellite. Secondly, checking that all the components stay within their operating temperature limits [7].

3.2.   The HERMES ESATAN model

The process of crating a thermal model of a CubeSat consists of many steps. The first one is to understand what can be considered relevant from a thermal point of view. These elements can be, for example, structural elements, dedicated pieces of electronics (like PCBs), panels, payloads and thermal solution devices. To identify all these components, the engineers focus their attention on the power dissipated, the thermal inertia, the optical properties and the connections with other elements of the satellite. Among all the thermophysical properties, the dissipated power and the thermal interfaces are considered to be critical. Once these components are identified, the next step consist in creating the element on the software. Here, especially at the early stages of the design, the thermally relevant components are simplified based on identification of the parts that have a large heat capacity, dissipate power, or have thermal connections between the components. As a matter of fact, the lack of thermal data on CubeSats such as conductive coupling between components leads to a large uncertainty on the outcome of the analysis. Moreover, it is not always clear what type of materials are used (and their purity), what the contact conductance is, or even the surface properties [8].

Fig. 3.1 shows the HERMES assembled model, with all the relevant thermal components. It can be noticed how the structural elements of the CubeSat are simplified and modeled as straight bars. Since their operative temperature window is quite wide, with respect to other critical components, their geometry can be approximated without compromising the simulation results. Moreover, in the initial assembled model, only the relevant elements of the other components are represented.

Once the model is complete, it is possible to run the preliminary analysis to assess the temperature fields in the worst hot and cold cases.
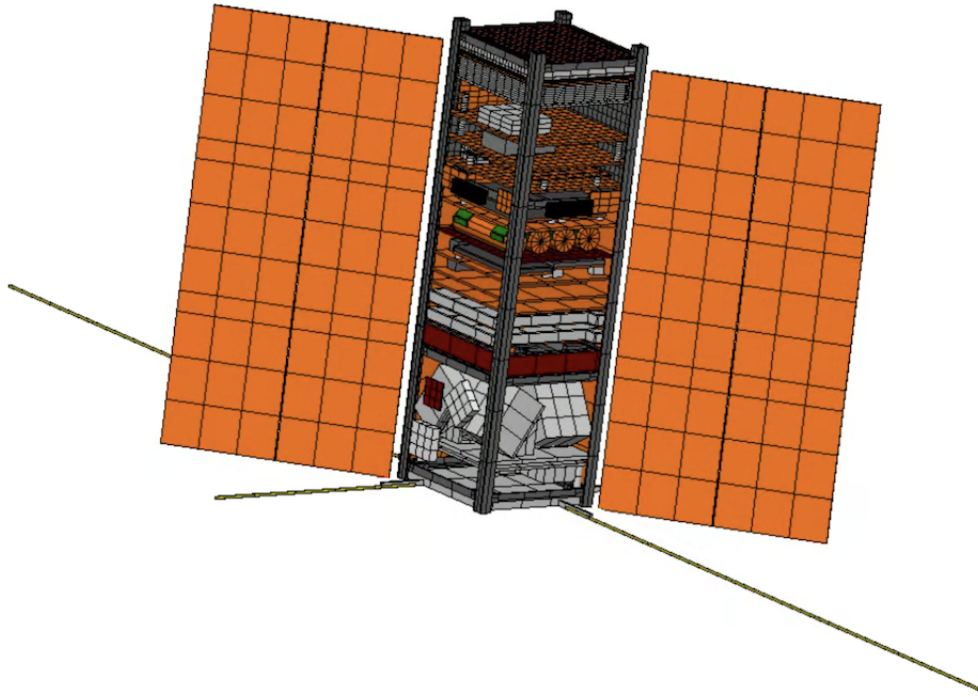
(a) HERMES assembled model front view.
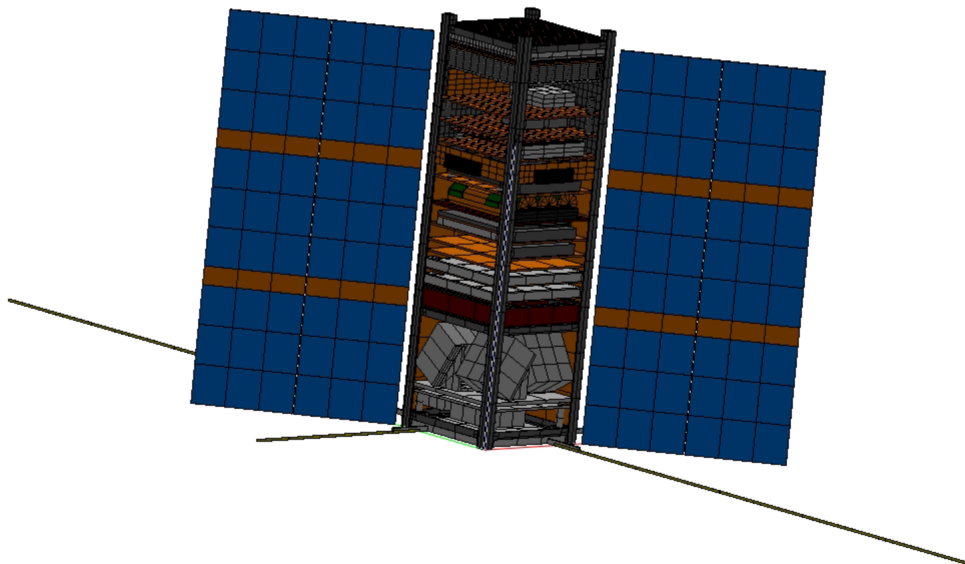
(b) HERMES assembled model back view.

Figure 3.1: HERMES assembled model, front and back views.

3.3.   The enhanced HERMES model

Let us now focus on the enhanced model of the battery and how it interacts with the other components. The enhanced model of the battery is made to study some critical situations. At this point of the thermal study, the results of the preliminary thermal analysis are already available. Since more information are available, the model is more detailed and the results of the simulation can be more reliable. The battery model interacts with the other components of the satellite mostly by irradiation. However, to simulate that the battery PCB is mechanically attached to the main structure of the satellite, four UDCs are used to physically connect the battery PCB to the underlying GPS package, and other four UDCs connects the battery to the above ADCS model. An example of the spacers is visible in Fig. 3.2.
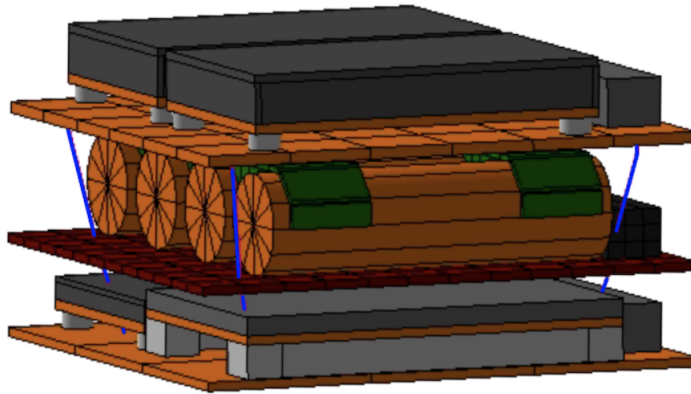
Figure 3.2: Blue spacers connecting the battery PCB to the other components of the satellite.

4 | The simulations

Once the model of the battery is finished and the connections with the rest of the satellite are set, only the settings of the simulation are required. The following chapter explains the conditions set for the different simulations. Moreover, the battery budgets and the data used during the simulations are showed. Finally the results are presented and compared with the ones obtained with the initial model.

4.1.   What types of simulations are carried out

The simulations are run to better analyze two conditions. These conditions coincide with two most power demanding modes that the satellite will enter during its mission. The two modes are the OBS and the COMM-DATA (more details in the following sections).

The results from the preliminary thermal analysis, in OBS and COMM-DATA mode, showed that the temperatures reached by the battery cells were close to the upper limits with a margin of less than 5 °C from the upper temperature limit. An example is reported in Fig. 4.1 and 4.2: all four battery cells are very close to the hot temperature limit. A better analysis is required to check that this safety margin is not further reduced.
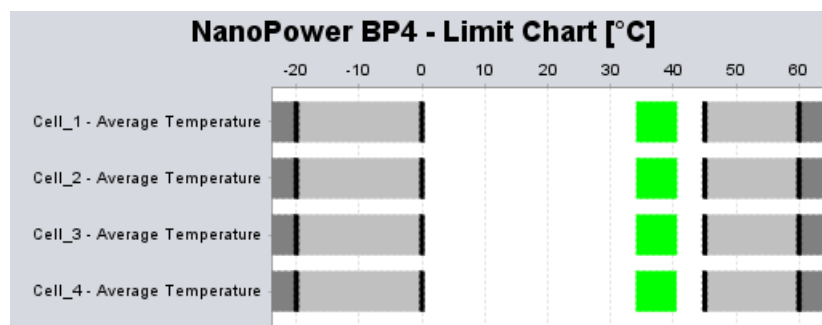
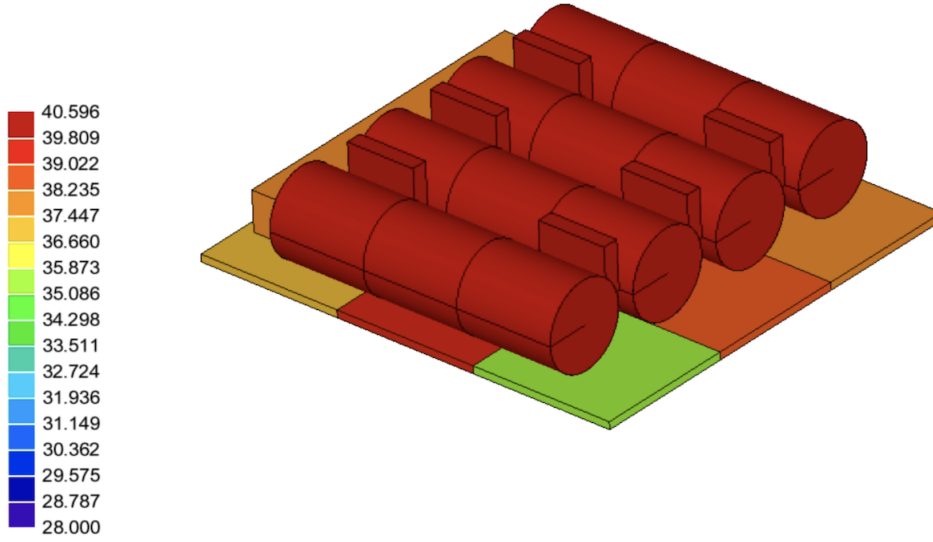Figure 4.1: Temperature limits of the 4 NanoPower BP4 cells.

Figure 4.2: NanoPower BP4 temperature evaluated at 2581 s, initial model

The goal of the simulations with the enhanced model is to understand if the temperatures reached are due to the approximations of the ESATAN model or due to the design. In particular, in the case the temperature reached by the batteries are confirmed by the new results, this would mean that the approximations performed during the initial modeling were correct from an engineering point of view. Thus, the initial model correctly represents the key elements from the thermal point of view and the results justify the design chosen for the mission. However, in the case of discrepancy between the old and the new results, this would mean that the initial approximations led to a wrong model of the reality and as a consequence the results are far from the real ones.

Let us now look at the set up for the simulations. For all the simulations, it is considered a zenith pointing circular, $e = 0$, orbit around the Earth with a semi-major axis, a, of 6871 km. The Earth radius is set to 6371 km, so the altitude of the orbit with respect to the Earth surface is 550 km. The inclination, i, the right ascension, Ω, the argument of periapsis, ω, and the initial true anomaly, θ, are all set to 0 deg, as summarised in Tab. 4.1.

a [km]	e	i [deg]	ω [deg]	Ω [deg]	θ [deg]
6871	0	0	0	0	0

Table 4.1: Orbital parameters.

For what concerns the environment, the Sun is considered to be at 1 au, its surface temperature, T_s, is set to 5778 K, while the environment temperature, T_{env}, is set to 3 K. Moreover, the solar declination, δ_s, is 0.19 deg, while the Sun right ascension, Ω_s, is 0.44 deg. Finally, the Earth temperature, T_e, the Earth albedo, A_e, and the Earth infra-red emission, Ψ_e, are considered to be equal to 254.3 K, 0.31 and 1, respectively, as reported in Tab. 4.2.

Sun distance [au]	T_s [K]	T_e [K]	Ω_s [deg]	δ_s [deg]	A_e	T_e[K]	Ψ_e
1	5778	3	0.44	0.19	0.31	254.3	1

Table 4.2: Environment parameters.

Moreover, since the solar panels can be considered relevant during the simulations from a thermal point of view, it must be pointed out how they are oriented. During the simulations, the satellite points the payload towards the zenith direction, while keeping the solar panels normal to the orbital plane. In order to catch most of the sunlight the AOCS makes the satellite rotate of 180° around the z axis, every half orbit. This way, the solar panels when exiting the eclipse are correctly oriented towards the Sun. The same goes for the other half orbit spent in the sunlight phase [7].
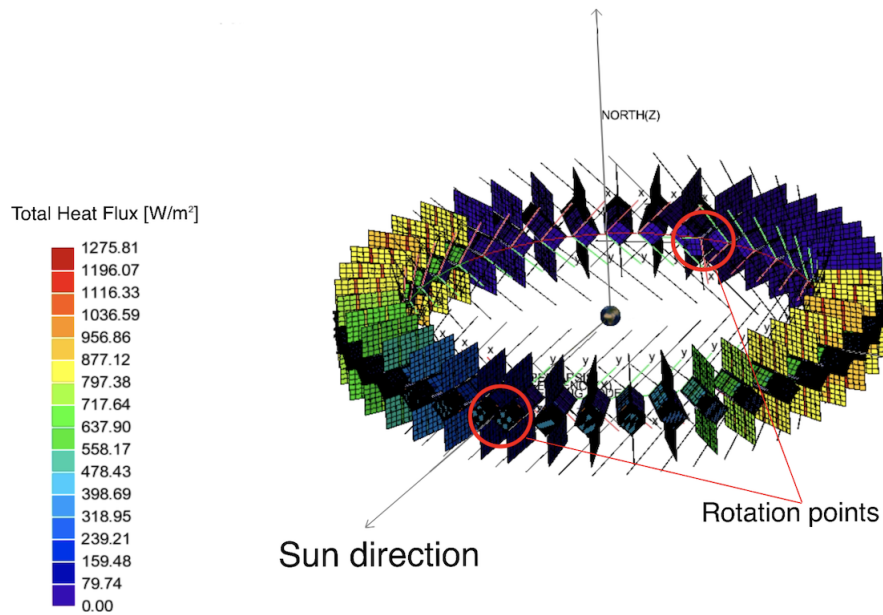

Figure 4.3: Solar panels orientation during the orbit.

Finally the solver setup. The setup are the same used during the initial analysis. Fig. 4.4
shows all the parameters set for the simulations. By doing so, the solver starts from the
steady state solution and cycle over 10 orbits (SOLCYC), plus in the end it computes
a final transient simulation (SOLCRNC), for a total of 11 orbits. The solvers uses the
Crank Nicolson method to solve the thermal problem with an initial time step (DTIMEI)
of 10 s and a maximum number of loops (NLOOP) set to 300.

```
C
        NLOOP=100
        RELXCA=0.01
        CALL SOLVFM
C
C
        TIMEND=5674.5767
        OUTINT=141.8644175
        NLOOP=300
        RELXCA=1.0E-4
        DTIMEI=10.0
        CALL SOLCYC('SLCRNC',0.01D0,0.01D0,5674.5767D0,10,' ','NONE')
C
        CALL SLCRNC
C
```

Figure 4.4: Solver settings.

4.2. Battery budget and data used during the simulations

Before showing the results of the simulations, it is required to display the thermal loads
generated by the payloads and the on-board components which are active during the
different modes of the satellite.

Let us start from the battery loads. In order to compute them, the charge-discharge profile
file was analyzed. This file included the information, as the current and the voltage of
the cells, about five charge-discharge cycles of the battery. In particular, the cycles were
simulating the performances of the battery during five consecutive orbits. As an input for
my simulations only the last cycle was considered. The choice to consider only the last
cycle was made to eliminate the possible transient effects that could affect the data. Once
the last cycle parameters were selected, it was possible to compute the power generated by
the batteries during the discharge phase and the power absorbed by the batteries during
the charge phase. Then, by means of the efficiency of the batteries, the thermal power
was computed. It is important to highlight that the efficiency of the batteries is different
during the charge phase, μ_c, and discharge phase, μ_d, as showed in Tab. 4.3.

Name	μ_c	μ_d
Battery	0.80	0.88

Table 4.3: Charge and discharge efficiencies.

Once the battery thermal power is computed, it is equally divided by four and used as the input for each cell. This load is displayed in Fig. 4.5.
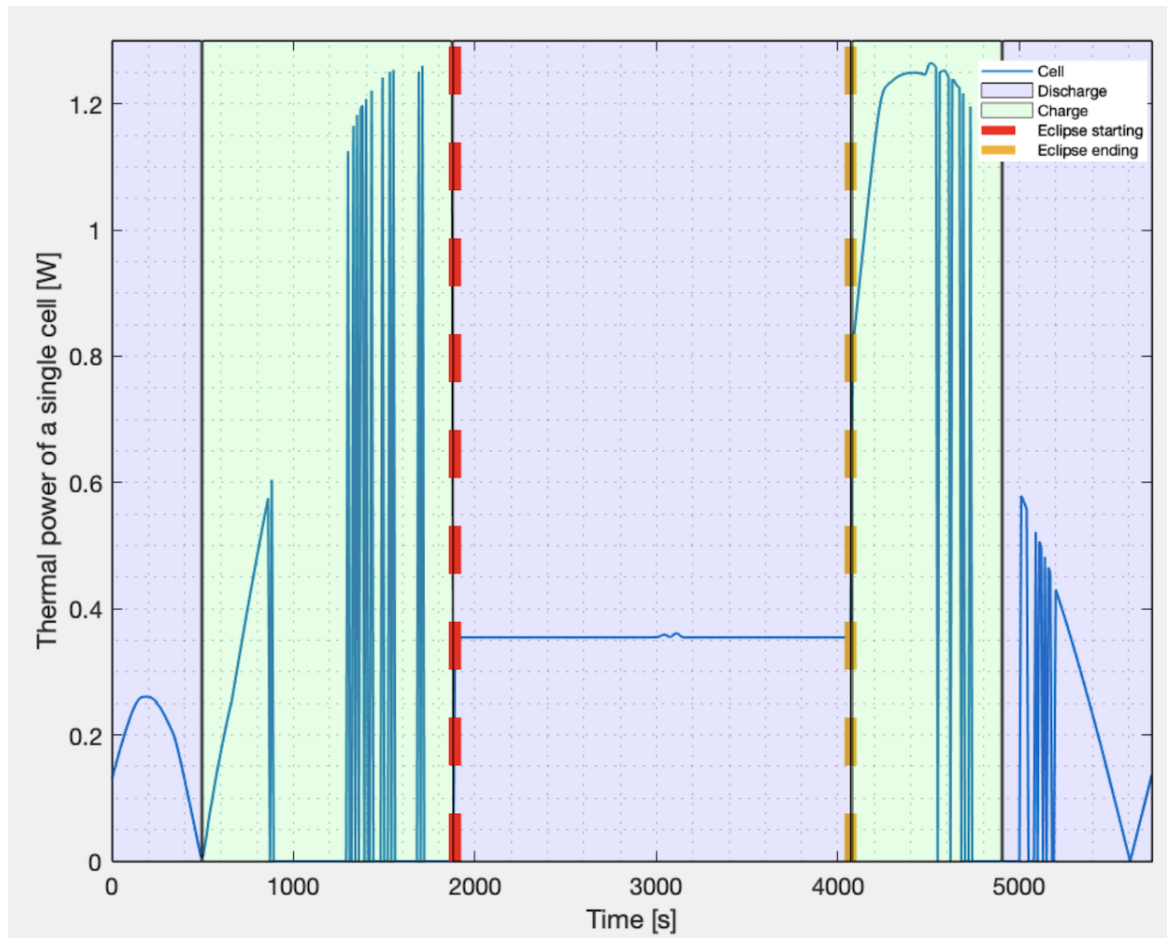

Figure 4.5: Thermal power dissipated by a single battery cell, OBS mode.

To compute the thermal loads generated by the other satellite components, the EPS power budget is used. The power budget in visible in Tab. 4.4, Tab. 4.5 and Tab. 4.6.

HERMES components	PDU Channels	Component margin	Avg Power mW	OBS	COMM DATA	COMM TC	MNVR	HSAFE	SSAFE
ACU	internal-V3,3	0,1	329	1	1	1	1	1	1
ANT-GPS	2	0,1	33	1	1	1	1	0	1
ANT-S	7	0,1	0	0	1	0	0	0	0
ANT-UHF	8	0,1	40	0	0	1	0	0	0
COMM-S	7	0,1	6000	0	1	0	0	0	0
CSS	1	0,1	324	1	1	1	1	1	1
GPS	2	0,1	1320	1	1	1	1	0	1
I-ETC	internal-V3,3	0,1	1162	1	1	1	1	1	1
IMU	4	0,1	850	1	1	1	1	0	1
IRIDIUM	5	0,1	247	1	0	0	0	0	0
MGMTR	2	0,1	8,3	1	1	1	1	1	1
MTORQ	2	0,1	400	1	1	1	1	0	1
OBC-ADCS	2	0,1	170	1	1	1	1	0	1
OBC-MAIN	internal-V5	0,1	1000	1	1	1	1	1	1
PDU	internal-V3,3	0,1	405	1	1	1	1	1	1
PL12	1	0,2	288	1	1	1	1	0	0
PL3	6	0,2	1214,4	1	1	1	1	0	0
PL5	0	0,2	415	1	1	1	1	0	0
RWL-ASM	3	0,1	800	1	2,5	1	2,5	0	1
SP	1	0,1	6670	0	0	0	0	0	0
SUNS-X	2	0,1	46,2	1	1	1	1	1	1
TRX-UHF	8	0,1	6000	0	0	0,32	0	0	0
			[W]	9,01	15,96	10,72	9,96	3,27	6,85

Table 4.4: Power budget, part 1.

HERMES components	BOOT	BOOT IRID	DTMB	DTMB UHF-TX	DTMB-UHF TX-RX	DTMB-UHF TX-RX-SAFE	SUN-UHF TX-RX	SAFE_UHF IRID_MAX
ACU	1	1	1	1	1	1	1	1
ANT-GPS	0	0	0	0	0	0	1	0
ANT-S	0	0	0	0	0	0	0	0
ANT-UHF	0	0	0	0,17	1	1	1	1
COMM-S	0	0	0	0	0	0	0	0
CSS	0	0	0	0	0	0	1	1
GPS	0	0	0	0	0	0	1	0
I-ETC	0	0	0	0	0	0	1	1
IMU	0	0	0	0	0	0	1	0
IRIDIUM	0	32,4	0	0	0	0	0	1
MGMTR	0	0	1	1	1	1	1	1
MTORQ	0	0	0,25	0,25	0,25	0,25	0,25	0,3
OBC-ADCS	1	1	1	1	1	1	1	1
OBC-MAIN	1	1	1	1	1	1	1	1
PDU	1	1	1	1	1	1	1	1
PL12	0	0	0	0	0	0	0	1
PL3	0	0	0	0	0	0	0	1
PL5	0	0	0	0	0	0	0	1
RWL-ASM	0	0	0	0	0	0	1	1
SP	0	0	0	0	0	0	0	0
SUNS-X	0	0	0	0	0	0	1	1
TRX-UHF	0	0	0	0,17	0,43	0,22	0,43	1
	1,90	9,91	2,01	3,02	4,65	3,37	9,19	12,57

Table 4.5: Power budget, part 2.

HERMES components	DEPL SARRAYS	DEPL UHF	MNVR LEOP	BATT SAFE	BATT CRITICAL	SUN_PTNG LOW_PWR	SUN_PTNG HIGH_PWR	COMM TTC
ACU	1	1	1	1	0	1	1	1
ANT-GPS	0	0	1	0	0	1	1	1
ANT-S	0	0	0	0	0	0	0	0
ANT-UHF	0	50	0	1	0	0	0	1
COMM-S	0	0	0	0	0	0	0	0
CSS	1	0	1	0	0	1	1	1
GPS	0	0	1	0	0	1	1	1
I-ETC	0	0	0	0	0	0	1	1
IMU	0	0	1	0	0	0	1	1
IRIDIUM	0	0	0	0	0	0	0	0
MGMTR	1	1	1	0	0	1	1	1
MTORQ	0,25	0,25	0	0	0	1	1	1
OBC-ADCS	1	1	1	0	0	1	1	1
OBC-MAIN	1	1	1	1	0	1	1	1
PDU	1	1	1	1	0	1	1	1
PL12	0	0	0	0	0	0	0	0
PL3	0	0	0	0	0	0	0	0
PL5	0	0	0	0	0	0	0	0
RWL-ASM	0	0	2,5	0	0	0	1	1
SP	1	0	0	0	0	0	0	0
SUNS-X	0	0	1	0	0	1	1	1
TRX-UHF	0	0	0	0,43	0	0	0	0,31
	9,01	4,01	6,49	4,37	0	4,04	6,85	8,76

Table 4.6: Power budget, part 3.

Depending on the satellite mode, the power budget shows what are the active loads associated to that mode. By summing the loads for each mode, it is possible to evaluate the modes which require more electrical power, as showed in the last raw of the power budget tables. Among those, there are the OBS and COMM-DATA modes, as visible in Tab. 4.4.

By closely look at them, it is possible to see that the active loads are more or less the same for the both of them. However, a big difference in the power required is generated by the COMM-S component. It must be said that, even if the load associated to the COMM-S component is relatively high (6W), it is expected to be active only during eclipse for a duration of 10 minutes.

Moreover, during all the simulations, a conservative choice is done. From the initial model simulations, it was noticed that the highest temperatures were reached during eclipse. Thus, the 10 minutes coinciding with the activation of the COMM-S component correspond to a critical time for the batteries from a thermal point of view.

Finally, another variable load in time is the one related to the reaction wheels.

4.3. Results comparison: initial model and enhanced model

In this section the results of the simulations are presented.

Let us start with the OBS simulations results. Fig. 4.6a and Fig. 4.6b show the temperature reached after 2270 seconds in the simulations. At this point, the temperatures reached are the highest during the orbit, as visible in Fig. 4.7 which shows the temperature profile of the four cells over a complete orbit of the satellite.
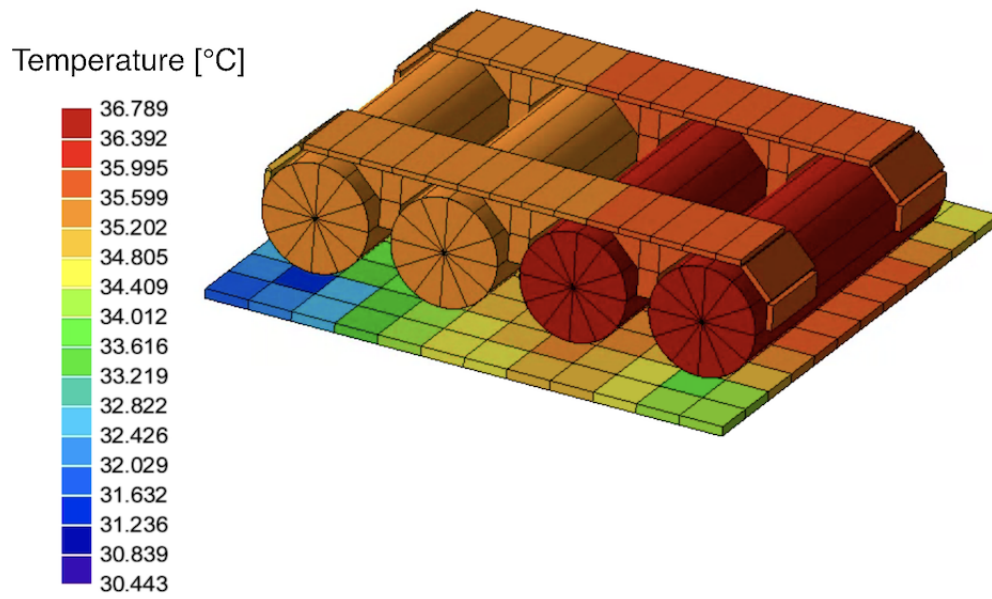
(a) Front view.
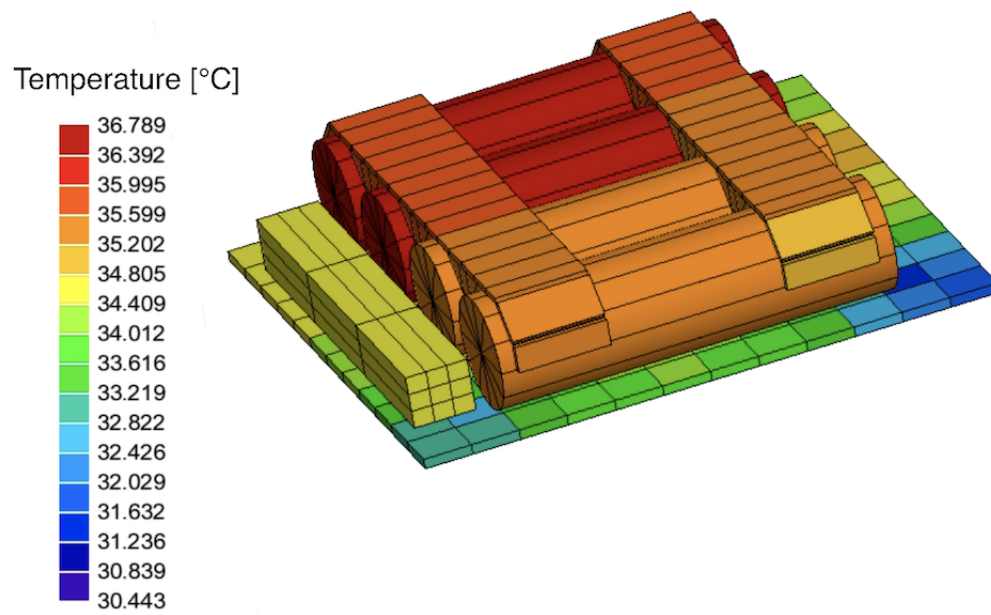
(b) Back view.

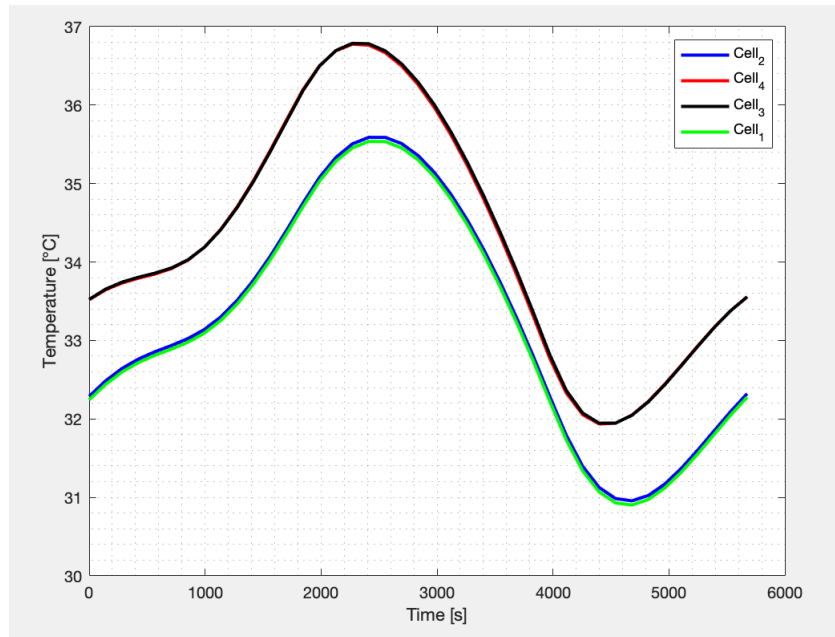Figure 4.6: Temperature results evaluated at 2270 s.

Figure 4.7: Cells temperature profile, OBS mode.

Moreover, it is possible to see from the limit chart, reported in Fig. 4.8, that the temperature limits are respected. The margins of the two cells with the higher temperature is relatively low, less than 10°C. However, it must be pointed out that the points where the cells temperatures are higher correspond to the point where the cells are discharging. As reported in Tab. 4.7, during the discharge phase the operational temperature window is wider with respect to the charge phase [1].
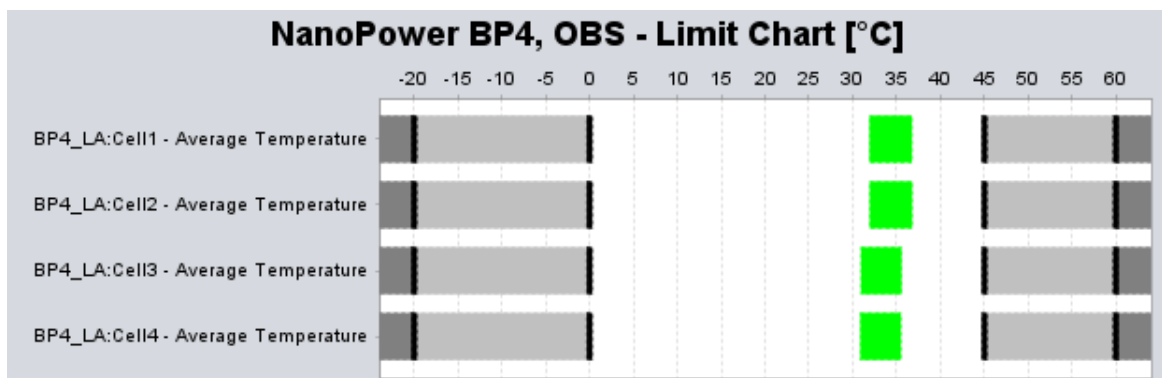
Figure 4.8: Cells temperature limit chart, OBS mode.

Parameter	Charge [°C]	Discharge [°C]
Operating Temperature	0, +45	-20, +60

Table 4.7: Charge and discharge operating temperature.

Finally, Fig. 4.9 shows the temperature profile of the hottest cell together with the operating temperature limits. On the plot, the region of the charge and discharge phases are highlighted by the green and lilac areas respectively.
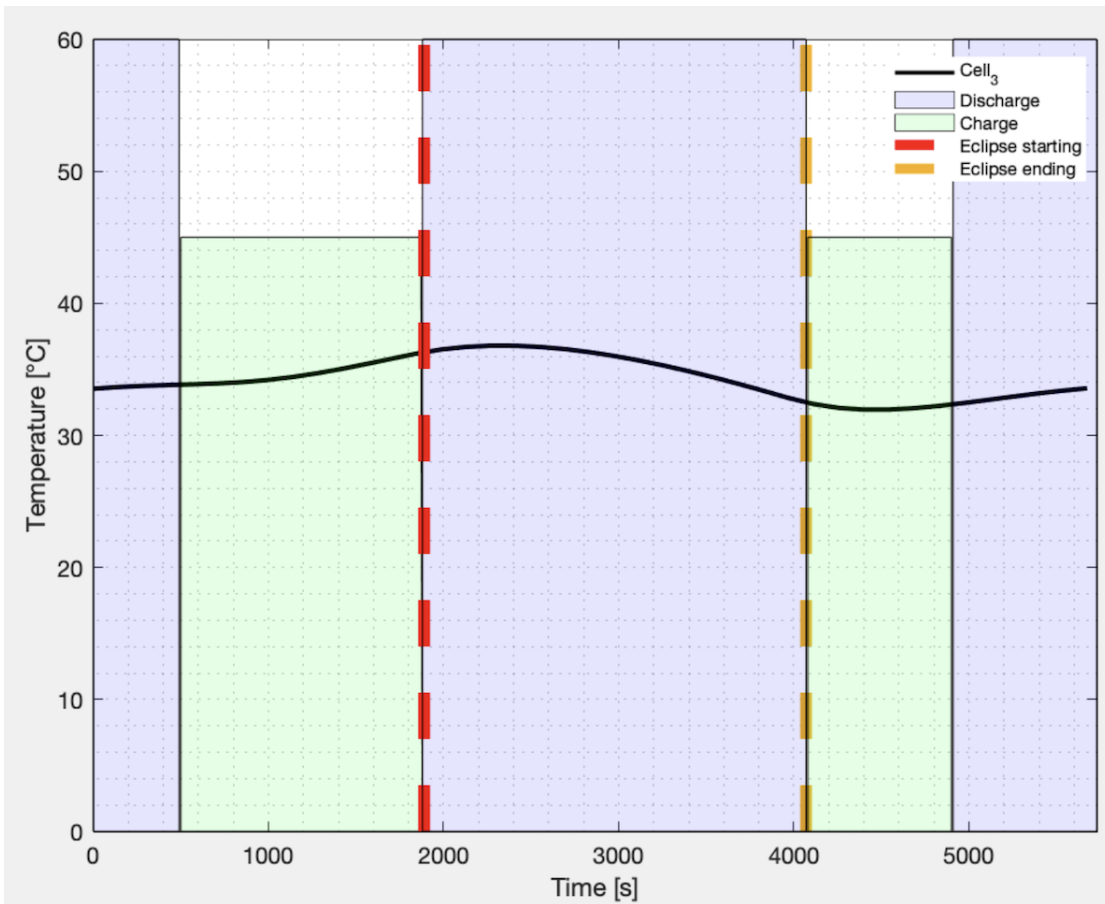

Figure 4.9: Cell temperature profile together with operative limits and eclipse region, OBS mode.

The red dotted line and the yellow dotted line in Fig. 4.9 represent the begin and end of the eclipse phase respectively. As a matter of fact, the eclipse region corresponds to a discharge phase of the battery. The other two discharge phases take place when the solar panels perform the rotation manoeuvre. Here, the direction of the plane of the solar panel forms an angle close to 90° with the direction of the Sun. This mean that a very

low amount of the solar radiation reaching the CubeSat can be converted into electrical energy. For this reason, to help the solar panel cover the required power by the on-board components, the batteries are discharging.

Let us now move to the results of the COMM-DATA simulation.

As reported in section 4.2, the thermal loads of the COMM-DATA mode are very similar to the OBS ones. However, this time it is also considered the load due to the COMM-S component. During this simulation, a conservative choice was made: the period of time when the COMM-S load is considered active coincides with the interval of time when the batteries will probably reach the highest temperature, as learned from the simulation ran with the initial model. This means that the temperature profiles of the batteries are going to show the worst hot case for the COMM-DATA mode.
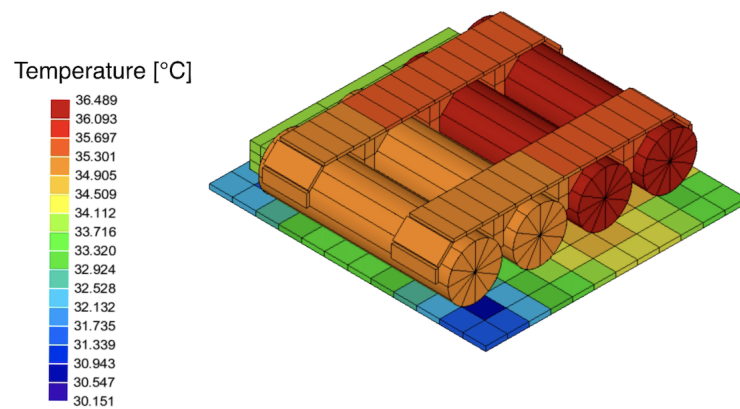
(a) Front view.
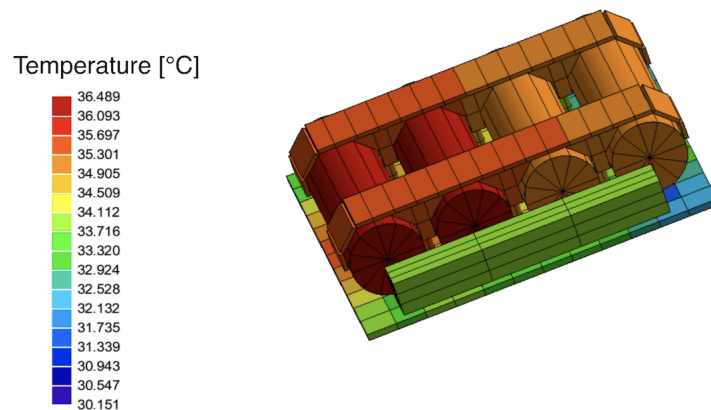
(b) Back view.

Figure 4.10: Temperature results evaluated at 2412 s.

Fig. 4.10a and Fig. 4.10b show the temperatures reached by the NanoPower BP4 components evaluated at 2412 s. The temperature of the cells, reported in Fig. 4.12, are similar to the OBS temperatures, and also in this case the temperature limits are respected, as visible in Fig. 4.11 .
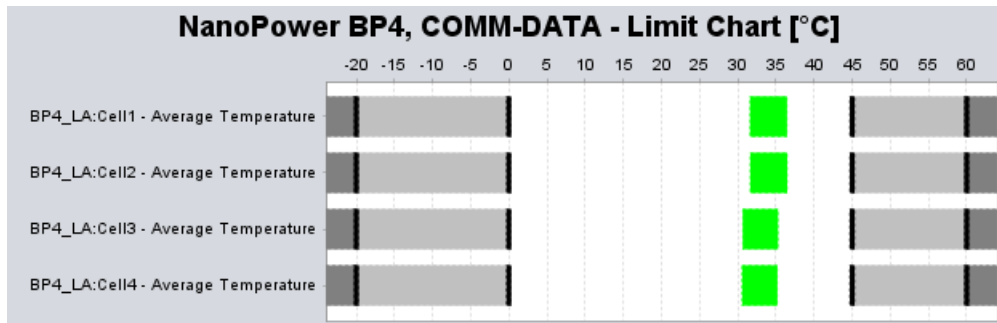

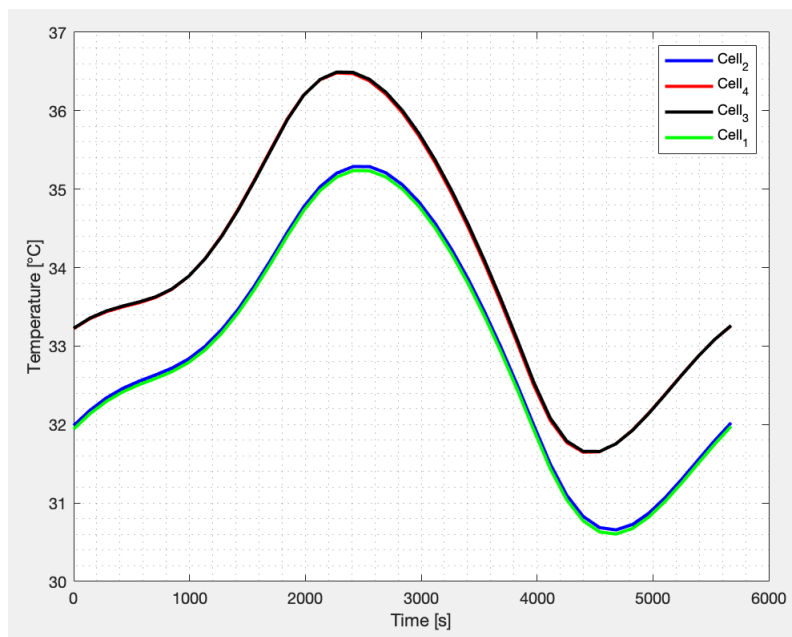Figure 4.11: Cells temperature limit chart, COMM-DATA mode.

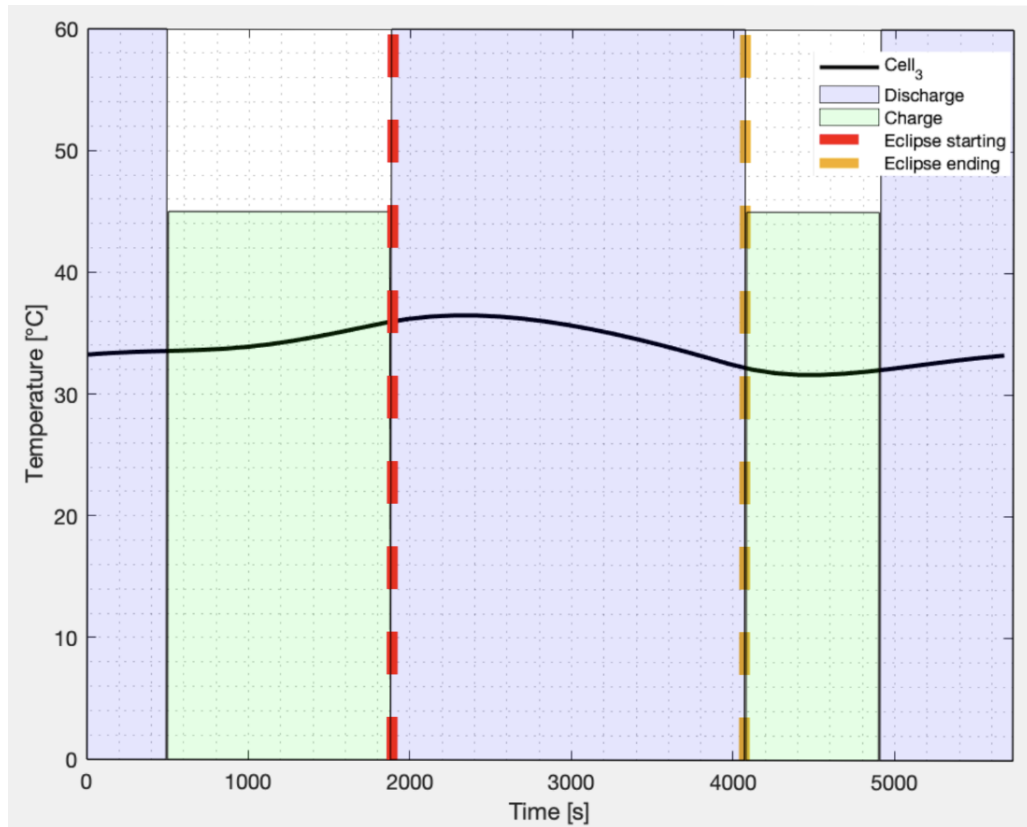Figure 4.12: Cells temperature profile, COMM-DATA mode.

Figure 4.13: Cell temperature profile together with operative limits and eclipse region, COMM-DATA mode.

Let us now compare the results of the enhanced model with the one of the initial model.

From the results of the simulations and from the limit charts, reported in Fig. 4.14 and Fig. 4.15 respectively, it can be easily noticed a difference: while in the reference model all the cells have the same temperature, in the enhanced model, two cells appear to be hotter than the others. It is clearly visible in the temperature profile plots reported in Fig. 4.7 and Fig. 4.12 that the temperature gap is almost constant for all the duration of the simulation. A possible reason to explain this temperature gap could be the differences in the meshes of the PCB in the models. Another possible option, could be the heat power generated by the GPS which is right below the batteries.

For what concerns the new results, the temperatures obtained with the enhanced model are even lower than the ones related to the initial model, as reported in Fig. 4.16.

This mean not only that the initial approximations were correctly performed by focusing on the key components from the thermal point of view, but also that a conservative analysis was carried out.
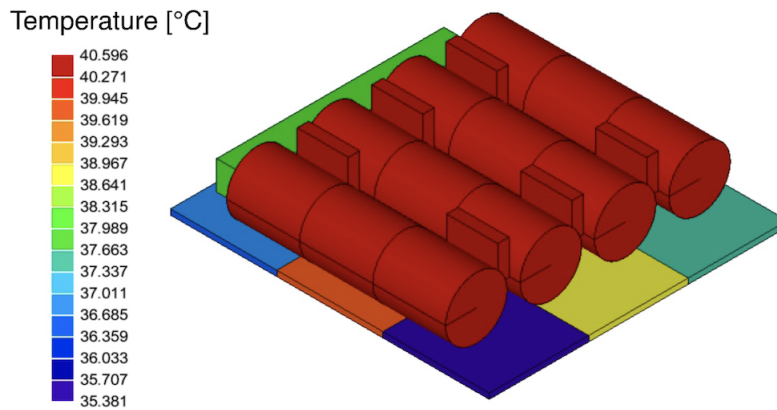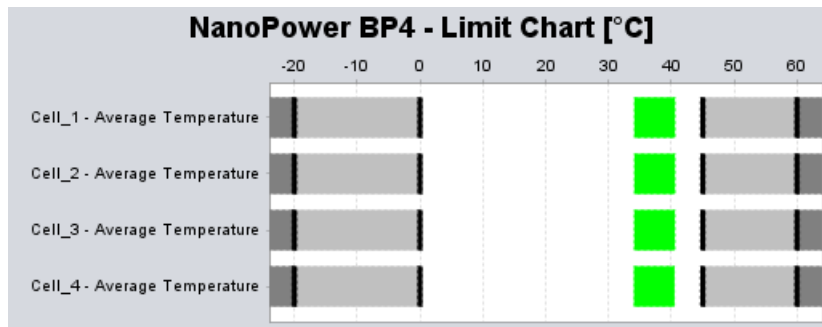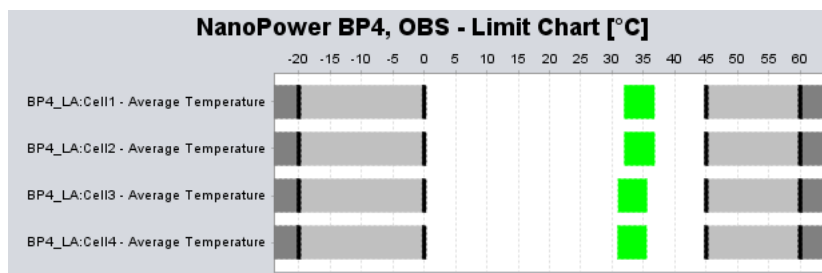
(a) Initial model.
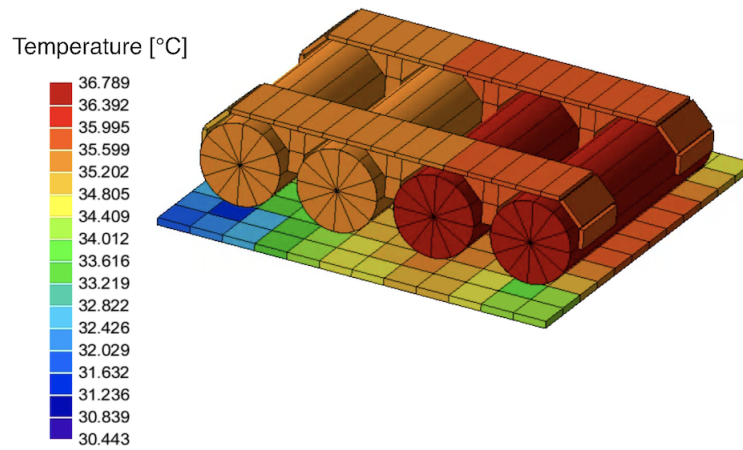
(b) Enhanced model.

Figure 4.14: Comparison: initial and enhanced models.

These results clearly answer the original question of the analysis performed: the temperature reached by the batteries in the initial model are the result of a well performed modelling phase. The model correctly represents the reality and the results justify the design chosen for the mission.

(a) NanoPower BP4, initial model.

(b) NanoPower BP4, enhanced model.

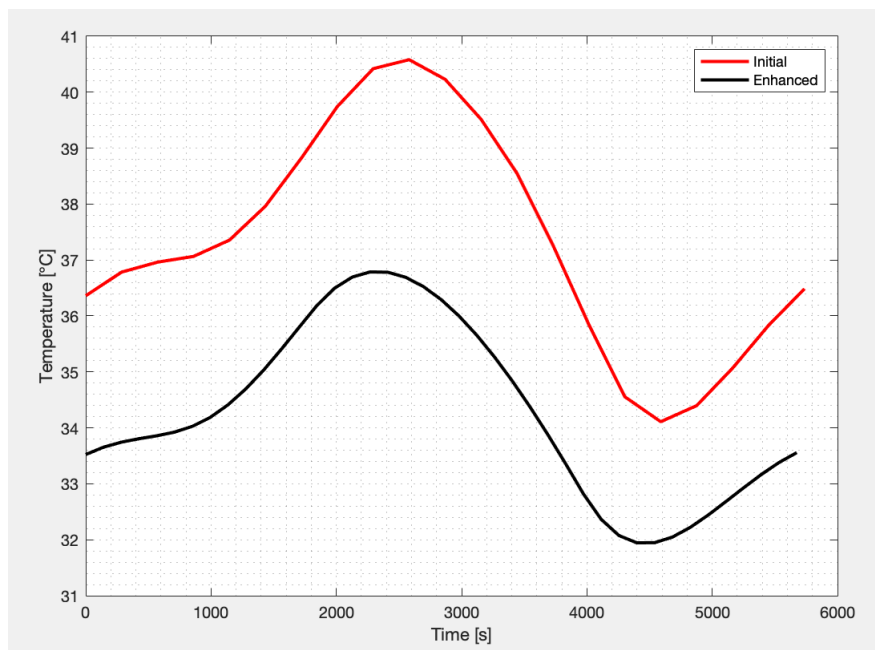Figure 4.15: Comparison: initial and enhanced model limit charts.

Figure 4.16: Comparison: initial and enhanced temperature profile, OBS mode.

5 | Conclusion and future work

5.1. Were the approximation affecting the results?

This analysis is performed to check that the initial approximations used to create the model in ESATAN were correct from an engineering point of view. If the model correctly represent the reality, it would lead to results that can be useful for the CubeSat mission. Otherwise, the model would misinterpret the reality and the results would lead to wrong information.

Once all the information regarding the external environment, the orbital parameters and the solver setup of the enhanced model are set, the analysis are performed to crosscheck the results of the initial model.

The results, although with some variations, show the same temperature trend and confirmed the accuracy of the initial model. This means that the key components were correctly modelled and that the approximation did not affect the results from a thermal point of view.

However, among the small differences in the results, there is the gap temperature between the two cells in the enhanced model, while in the initial model all the cells have the same temperature. In this case, a possible reason to it could be the meshes differences in the battery PCB together with the heat flow coming from the GPS, collocated right below the batteries.

5.2. Possible solutions to heat management

Regarding the gap temperature problem, it should be demonstrated that it is due to the heat flowing from the GPS box. In order to prove this, a simulation without the mechanical components (spacers) linking the battery PCB to the GPS box could be run. This way, only a radiative heat exchange will take place. If this is true, a possible solution to manage the temperature of the cells, could be to apply a layer of MLI in a position beneath the battery PCB corresponding to the position where the two hot cells

are collocated. By doing so the heat exchange with the GPS will be mitigated. However, in this case the GPS box would heat up. It must be checked that it remains inside its temperature limits. Another possible option could be to use the temperature margins of other components by creating a mechanical connection between the hotter cells and the colder components. By doing so, the other components would be used as thermal sinks. Both these solutions are passive solutions, which are typically used in CubeSat heat management.

5.3.   Next work: sensitivity analysis and validation

Finally, especially for what concerns UDCs and CIs, a sensitivity analysis should be carried out. These parameters are the one with the higher uncertainties since they are difficult to represent in the model and it is also complicated to have reliable information about their thermal properties through experiments.

The sensitivity analysis would be used to check how these components affect the results and how a variation of their thermal properties can change the simulation results.

A further step could also be to perform tests in laboratories. By reproducing the conditions used during the simulations and using real components, more information could be gathered in order to correlate and validate the models and the simulation results.

Bibliography

[1] G. A/S. Nanopower bp4, 2018. URL `https://gomspace.com/shop/subsystems/power/nanopower-bp4.aspx`.

[2] G. A/S. Nanopower bp4 datasheet, 2018. URL `https://gomspace.com/UserFiles/Subsystems/datasheet/gs-ds-nanopower-bp4-27.pdf`.

[3] H. Curtis. Satellite batteries – for cubesats, nanosats, and other form factors, 2021. URL `https://blog.satsearch.co/2021-06-23-satellite-batteries-for-cubesats-nanosats-and-other-form-factors`.

[4] P. Hager, T. Flecht, K. Janzer, L. Leon Perez, H. Brouwer, and M. Jonsson. Contact conductance in common cubesat stacks. 49th International Conference on Environmental Systems, 2019.

[5] V. Knap, L. K. Vestergaard, and D.-I. Stroe. A review of battery technology in cubesats and small satellite solutions. *Energies*, 13(16):4097, 2020.

[6] F. Miglietta. *Elementi di FISICA TECNICA*. Pitagora Editrice Bologna, 2015.

[7] M. Quirino. Thermal analysis of hermes-tp cubesat using esatan and openfoam, 2019. URL `http://hdl.handle.net/10589/151674`.

[8] A. K. te Nijenhuis, H. S. Brouwer, M. Jonsson, R. C. van Benthem, E. A. Bloem, and B.-J. Vollmuller. Thermal modelling of cubesats in esatan-tms: A modular approach. 2020 International Conference on Environmental Systems, 2020.